Available online at www.sciencedirect.com
SCIENCE DIRECT®
ELSEVIER
Earth and Planetary Science Letters 212 (2003) 407–416
EPSL
www.elsevier.com/locate/epsl

A network model for permeability in partially molten rocks

Wenlu Zhu *, Greg Hirth

Department of Geology and Geophysics, Woods Hole Oceanographic Institution, Woods Hole, MA 02543, USA

Received 7 October 2002; received in revised form 5 May 2003; accepted 9 May 2003

Abstract

Estimation of permeability in partially molten rocks requires knowledge of the melt phase distribution at the grain-scale. The melt distribution in an isotropic two-phase (solid+melt) system under equilibrium conditions is well defined. In such a system, all of the melt channels are identical and they are either interconnected or isolated depending upon the dihedral angle and the melt fraction. A simple power-law relationship between permeability, grain size and melt fraction has been derived for such a system. However, several factors, such as non-hydrostatic stress, anisotropic interfacial energy, or the existence of a third phase, will alter this relationship. We developed a three-dimensional network model to calculate permeability as a function of melt fraction for a system with a distribution of dihedral angles. In our model, each channel is treated as a prism with a length of the grain edges. The cross-sectional area of each prism is determined by a given dihedral angle and a melt fraction. By incorporating different dihedral angles into a network model, we are able to model permeability of partially molten rocks, taking the grain-scale heterogeneity of melt distribution into account. Our results show that the permeability of a heterogeneous system can be significantly smaller than the calculated permeability of an isotropic system with the same median dihedral angle.

Keywords: partially molten rocks; dihedral angle; melt fraction; network model; permeability; grain-scale heterogeneity

1. Introduction

The chemical and physical properties of partially molten regions of the crust and mantle are strongly influenced by the amount of melt present, and therefore the rate of magma segregation. Our current understanding is that melt migration in a typical mantle rock resembles fluid flow in a porous medium, and permeability is an intrinsic rock property that controls the flow rate (i.e. Darcy's law). At high melt fraction ϕ (say, $\phi > 0.05$), melts form an interconnected network and permeability is controlled by the effective size of melt channels. At low melt fraction ($\phi < 0.05$), however, the connectivity of melts is determined by the surface tension of solid–melt interfaces. In this case, whether melt channels are interconnected or isolated plays the most important role in melt migration processes. Estimation of permeability requires detailed knowledge of the grain-

* Corresponding author. Tel.: +1-508-289-3355; Fax: +1-508-457-2103.
E-mail addresses: wzhu@whoi.edu (W. Zhu), ghirth@whoi.edu (G. Hirth).

0012-821X/03/$ – see front matter © 2003 Elsevier Science B.V. All rights reserved.
doi:10.1016/S0012-821X(03)00264-4

scale distribution of melt, including dihedral angles, melt fraction, and the size of melt channels [1–9].

In a partially molten system with one solid phase and isotropic interfacial energy, chemical and mechanical equilibrium requires a constant mean curvature of solid–melt interfaces and a constant dihedral angle [7]. In such a system, if the dihedral angle is less than 60°, an interconnected network of melt channels forms along the grain edges and melt migration is feasible even at very low melt fractions. If the dihedral angle is greater than 60°, isolated melt pockets form at the grain corners and melt is immobile unless a critical melt fraction is exceeded [1,3,10,11]. Quantitatively, the permeability k of such a system can be expressed as a function of melt fraction ϕ, grain size d, and geometrical factor C [7,12–14]:

$$k = \frac{\phi^2 d^2}{C} \tag{1}$$

The power law of $k \propto \phi^2$ is consistent with the permeability–porosity relationship predicted for an array of identical tubes [15]. For convenience, we use porosity and melt fraction interchangeably throughout this paper.

Microstructural observations on texturally equilibrated partially molten rocks reveal that the melt distribution is more complex than predicted by the isotropic model [9,16–20]. For example, Waff and Faul [8] demonstrate that textures in experimentally produced aggregates of olivine and basaltic melt consist of both smooth curved solid–melt boundaries predicted by the isotropic equilibrium theory, and a considerable number of flat solid–melt interfaces. Quantitative analysis of the melt distribution indicates that tubular melt channels along triple junctions coexist with disk-shaped melt inclusions on two-grain boundaries [9,20].

To estimate permeability of a system with grain-scale heterogeneity, Wark and Waston [21] adopted an experimental approach. In their experiments, monomineralic aggregates of quartz can be used as an analog for texturally equilibrated mantle rocks. Based on the laboratory measurements on the quartz aggregates with porosity ranging from 0.6 to 17%, they proposed an empirical permeability–porosity relationship:

$$k = \frac{\phi^3 d^2}{C} \tag{2}$$

The difference in the exponent of the power law translates into more than an order of magnitude difference in permeability at $\phi < 0.01$ [21]. Resolution of this discrepancy between the model prediction and laboratory observations has important implications for interpreting both geochemical constraints on the composition of basalts [22] and seismic velocities in partially molten regions of the mantle [23,24].

The deviation of the empirical results from the theoretical prediction is not surprising because grain-scale heterogeneities were not included in the theoretical model. Experimental measurements provide a useful approach for quantifying the physical properties of partially molten rocks [21]. However, because the permeability–porosity relationship was determined from curve fitting in most of the experimental studies, the value of the exponent itself reveals little of the physics of melt transport. Therefore, it is desirable to develop a model relating macroscopic permeability to the microscopic melt distribution, taking into account the grain-scale heterogeneity caused by anisotropic surface energy. Such a model will help us to better understand the experimental data. Furthermore, larger uncertainties involved in permeability measurements of low-porosity samples make it difficult to determine the permeability–porosity relationship at $\phi < 0.03$ [21]. However, to interpret the implications of geochemical data, one needs to estimate melt segregation rate at very low porosities, perhaps as low as 0.001 [25]. Since it is difficult to even generate samples with porosity less than 0.005, modeling efforts provide a complementary approach to this problem. In this study, we use a numerical approach to calculate permeability of partially molten rocks. Specifically, a three-dimensional (3D) network model based on percolation theory is employed. This approach allows us to link the topology of melt phases and the geometry of individual melt channels to the bulk physical properties. The strength of our approach is that we can quantify

the effects of grain-scale heterogeneities on melt transport by explicitly incorporating the distribution of melt (including melt topology, connectivity etc.) in the network models.

2. A network model

A porous rock can be modeled using a 3D network, in which the conducting elements resemble the randomly assigned pore space. Combined with accurate pore structure statistics, such networks have been used successfully to predict permeability [26–30]. A network model is different from a simple channel model, such as the one illustrated by Turcotte and Schubert [15], in that the latter does not account for how different tubes are interconnected [31].

Isotropic equilibrium theory predicts that melt is distributed along the three-grain edges (i.e. triple junctions) and four-grain corners (i.e. quadruple junctions) of tetrakaidekahedral grains of equal size (Fig. 1) [1]. The shape of melt channels

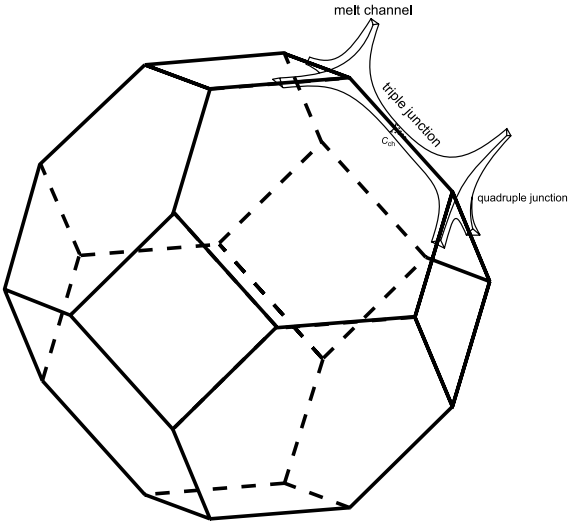

Fig. 1. A schematic diagram of a tetrakaidekahedron grain. It has 14 facets, including six squares and eight hexagons, 24 corners, and 36 edges. In a texturally equilibrated partially molten system, melt resides at the grain corners (quadruple junctions) and edges (triple junctions). A melt channel is superposed at one grain edge. The shape of the melt channel (the minimum cross-sectional area C_{ch}) is determined by both the dihedral angle and the melt fraction [7].

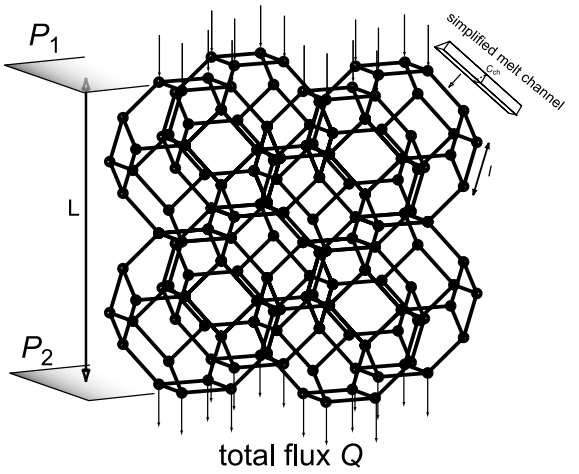

Fig. 2. A schmetic diagram of a 3D tetrakaidekahedron network model. In this model, each grain corner has four grain edges connected to it, corresponding to a coordination number of 4, except at the network boundaries. The conducting bonds are triangular prisms with cross-sectional areas equal to the minimum cross-sectional area C_{ch} of the melt channels. The flow through the model is driven by an imposed pressure gradient (P_1-P_2).

and the way they join at four-grain corners is a complex problem itself. Von Bargen and Waff [7] show that the geometry of the channel is such that the minimum cross-sectional area C_{ch} of the channel is located in the middle of a three-grain junction (triple junction). In this study, we build a 3D network model based on such grain shapes and melt channel geometry (Fig. 2). We used a model size of $14\times14\times14$ unit cells (1 unit cell = 1 tetrakaidekahedral grain, see Fig. 1), which corresponds to a total of 65 804 bonds (i.e. melt channels). This network is large enough that boundary effects can be neglected. Each bond in Fig. 2 represents a simplified melt channel. Each of the melt channels is connected to three other channels at a four-grain corner.

Von Bargen and Waff [7] demonstrated that permeability of a partially molten system is primarily controlled by the minimum cross-sectional area C_{ch} (Fig. 3 of this paper, see also figures 9 and 15 in von Bargen and Waff [7]). We adopt a simplified geometry for each conducting bond (melt channel) in the network: a triangular prism with a cross-sectional area equal to the minimum cross-sectional area C_{ch} of a melt channel with a

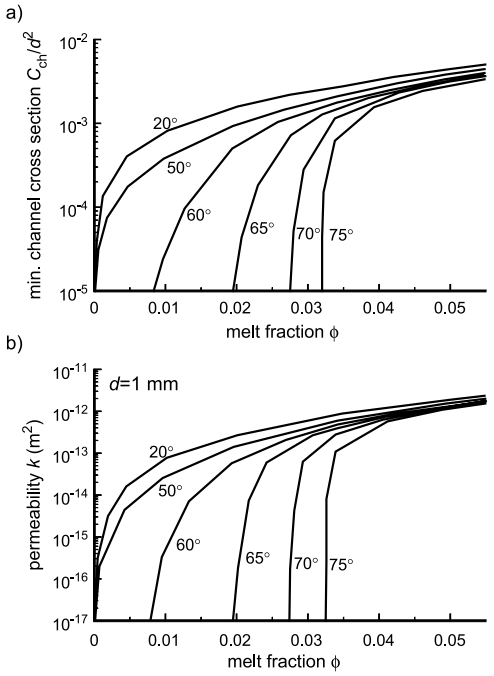

Fig. 3. (a) Normalized minimum channel cross-sectional area, and (b) bulk permeability versus melt fraction. (Results from von Bargen and Waff [7].) Each curve represents a system with a single dihedral angle (marked next to the curve). The two trends closely track each other, which indicates that the permeability of a texturally equilibrated partially molten rock is primarily controlled by C_{ch}.

given melt fraction and dihedral angle. We further assume that the quadruple junction corners exert no resistance to the flow. Given a distribution of dihedral angles and the local melt fraction, the cross-sectional area C_{ch} can be obtained from von Bargen and Waff [7]. The hydraulic conductance g_h of a simplified melt channel can then be expressed as:

$$g_h = \frac{1}{20\sqrt{3}} \frac{C_{ch}^2}{l} \tag{3}$$

where l is the length of the melt channel. In a regular tetrakaidekahedron:

$$l = \sqrt{2}d/4 \tag{4}$$

where d is the grain size, which is defined as the length between one square face to the opposite square face (Fig. 1). The heterogeneity of this network is determined by the distribution of the local hydraulic conductances g_h of the melt channels. The values of g_h, which are determined by the mean dihedral angles and the local melt fraction, are randomly distributed to melt channels in a network. We recognize that because the melt channels are located at triple junctions, the distribution of these channels is not completely random, but locally 'correlated'. However, our preliminary simulation results in a two-dimensional square network suggest that the 'local correlation' has little effect on the bulk permeability of the network. To reduce the computation time, the random distribution was employed in this study. Because of the sufficiently large size of our model, the fluctuation caused by the random distribution is small [27].

When constant pressures P_1 and P_2 are applied to the two parallel boundaries of the network (Fig. 2), the pressure gradient across the network is the driving force for melt transport. Because the distribution of the local hydraulic conductance is heterogeneous, the pressure at each node can vary significantly. The flow rate through each channel can be calculated using simultaneous equations for the nodal pressures derived by assuming Poiseuille flow in each channel and mass conservation at each node. Once the total flux Q is determined, the macroscopic conductance (bulk permeability) for the random network can be calculated. More technical details about this calculation can be found in Zhu et al. [27].

The average of the cross-sectional area square $\langle C_{ch}^2 \rangle$ can be calculated using Darcy's law:

$$Q = \frac{\langle C_{ch}^2 \rangle}{\mu} \frac{P_1 - P_2}{L} \tag{5}$$

where μ is the viscosity of the melt, and L is the distance between the two parallel boundaries (Fig. 1; in a $14\times14\times14$ network model, $L = 14d$). The bulk permeability k is then determined using the averaging scheme proposed by Guéguen and Dienes [32]:

$$k = \frac{1}{80\sqrt{3}} \frac{\langle C_{ch}^2 \rangle}{\langle C_{ch} \rangle} \phi \tag{6}$$

where $\langle C_{ch} \rangle$ is the average of the cross-sectional area C_{ch}.

To test the model, we first calculate the perme-

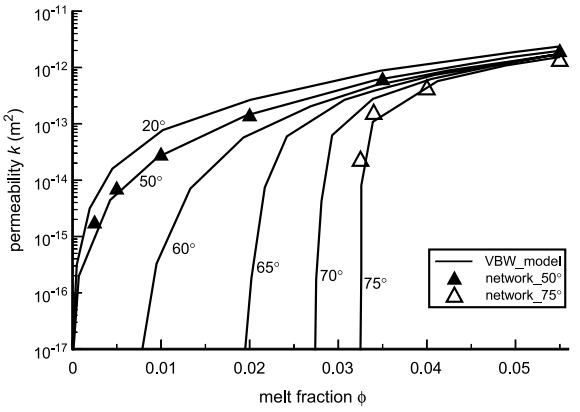

Fig. 4. Comparison of our simulation results for an isotropic two-phase system to von Bargen and Waff's calculations. The curves marked 20°–70° are results from von Bargen and Waff's study, where variations of the cross-sectional area along the individual melt channel were included [7]. The triangles are our simulation results using network models with a simplified channel geometry. The filled triangles represent data for a rock with dihedral angle of 50° and the open triangles represent data for a rock with dihedral angle of 75°. The agreement between our data and von Bargen and Waff's results indicates that the network model approach with simplified melt channel geometry is justified.

ability for a partially molten system with isotropic interfacial energy and one solid phase (i.e. a constant dihedral angle and uniform melt channels throughout the network). We used different combinations of dihedral angles (50° and 75°, respectively) and melt percentages (0.25–5.5%) in the calculations. As illustrated in Fig. 4, our simulation results show excellent agreement with those of von Bargen and Waff [7], despite the fact that we used a simplified channel geometry in the network models, whereas variations of the cross-sectional area along the individual melt channel were included by von Bargen and Waff [7]. We conclude that our network with simplified melt channel geometry is sufficient to study permeability of a partially molten system.

3. A simple three-phase system

Most upper mantle rocks have at least two major mineral components: olivine (ol) and orthopyroxene (opx) (i.e. harzburgites with 20–40% orthopyroxene). The average melt–solid dihedral angle of olivine is ~35° (from Waff and Bulau [2]), whereas the average melt–solid dihedral angle of orthopyroxene is ~75° (from Toramaru and Fujii [18]). This difference in dihedral angle inevitably results in a heterogeneous melt distribution. We demonstrate here how permeability is influenced by varying proportions of orthopyroxene in a mantle rock containing two solid phases: olivine and orthopyroxene. However, these results can be generalized to any three-phase system.

There are four possible configurations of triple junctions in such a system: ol–ol–ol, ol–ol–opx, opx–opx–ol, and opx–opx–opx (Fig. 5). The probability for each configuration to occur is determined by the ratio of olivine and orthopyroxene contents and the grain-size distribution in the mixture. Three cases are studied here with olivine:orthopyroxene = 4:1, 3:2, and 2:3, respectively (Table 1). In all three cases, we assume uniform grain size to isolate the effect of different dihedral angles on permeability.

To calculate the dihedral angle θ at an ol–opx–melt junction (Fig. 5e), we assume that the variation of interfacial energy with respect to orienta-

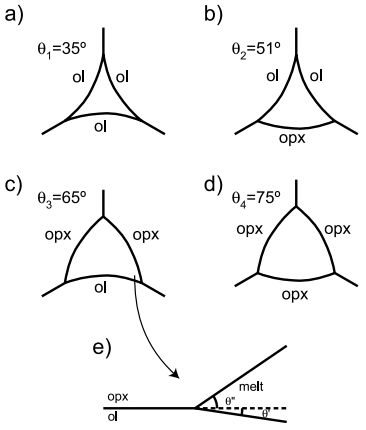

Fig. 5. Schematic diagram of the four possible configurations of triple junctions in a olivine+basalt system containing orthopyroxene: (a) ol–ol–ol; (b) ol–ol–opx; (c) opx–opx–ol; and (d) opx–opx–opx. (e) The dihedral angle θ at the anisotropic junction of ol–opx–melt is ~60°, which is determined by the solid–fluid interfacial energies and the grain boundary energy (see text for details). The effective dihedral angles of these four triple junctions are 35°, 51°, 65°, and 75°, respectively.

tion induced by the orthopyroxene addition to an olivine–melt system can be ignored [1]. Under this assumption, the dihedral angle θ is simply determined by the solid–fluid interfacial energies γ_{ol-m} and γ_{opx-m}, and the grain boundary energy γ_{ol-opx} [33,34]:

$$\gamma_{ol-m}\cos\theta' + \gamma_{opx-m}\cos\theta'' = \gamma_{ol-opx}$$
$$\gamma_{ol-m}\sin\theta' - \gamma_{opx-m}\sin\theta'' = 0 \quad (7)$$

where $\theta = \theta' + \theta''$ (Fig. 5e). Our calculation shows that $\theta \approx 60°$ at the junction of ol–opx–melt. Taking a simple average of the dihedral angles at a triple junction, the effective dihedral angles (θ_{eff}) of ol–ol–opx and ol–opx–opx are $\sim 51°$ and $\sim 65°$, respectively (Fig. 5).

At a given melt fraction, the minimum cross-sectional area C_{ch} for the four different triple junctions is determined using the results of von Bargen and Waff [7]. By creating a random distribution of channels with different C_{ch} in a 3D network model, we can calculate the bulk permeability of a three-phase mantle rock made up of olivine, orthopyroxene and melt. Our simulation results are shown in Fig. 6. The permeability calculated for the rock with 80% olivine and 20% orthopyroxene, which has a median dihedral angle of $\sim 44°$, is consistent with that predicted for an isotropic system with similar dihedral angle (i.e. a little less than 50°). In the rock made up of 60% olivine and 40% orthopyroxene, there are significantly more junctions with effective dihedral angles greater than 60° compared to that in a rock containing only 20% orthopyroxene (Table 1). Specifically, there are 6.4% opx–opx–opx triple junctions with $\theta_{eff} \approx 75°$ and 28.8% ol–opx–opx triple junctions with $\theta_{eff} \approx 65°$.

According to von Bargen and Waff [7], pinch-off (i.e. the melt fraction at which channels become isolated and therefore have no contribution to permeability) for junctions with effective dihedral angles of 75° and 65° occurs when $\phi < 0.03$ and $\phi < 0.02$, respectively. Our results in Fig. 6 show that, as melt fraction decreases from 0.05 to 0.01, the decrease in connectivity results in greater decrease in the permeability of a rock with 60% olivine than that predicted for the rock with 80% olivine. Interestingly, at melt fractions below 0.01, in the 60/40 system which has a median dihedral angle of $\sim 53°$, the permeability–porosity trend is similar to that of the 80/20 mixture. Notice that in Fig. 7, at high melt fraction (> 0.04), the slopes of permeability–porosity trends for all of the three mixtures are quite similar. This observation indicates that the permeability is insensitive to variations in dihedral angle when melt channels are interconnected [7] and that the connectivity loss exerts the primary control in melt transport. The difference in permeability between the heterogeneous three-phase system and the isotropic two-phase system becomes

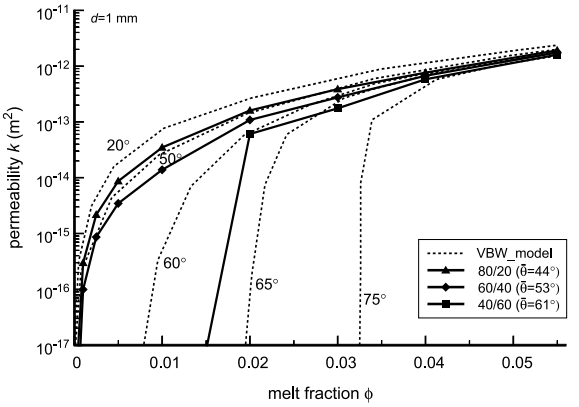

Fig. 6. Permeability as a function of melt fraction in three-phase systems. The solid curves with triangles, diamonds and squares represent calculations for olivine+basalt systems containing 20%, 40% and 60% orthopyroxene, respectively. For reference, the permeabilities calculated for an isotropic two-phase system by von Bargen and Waff are shown as dashed curves.

Table 1

Olivine content (%)	ol–ol–ol ($\theta_{eff} \approx 35°$)	ol–ol–opx ($\theta_{eff} \approx 51°$)	ol–opx–opx ($\theta_{eff} \approx 65°$)	opx–opx–opx ($\theta_{eff} \approx 75°$)	median dihedral angle $\bar{\theta}$ (°)
80	51.2%	38.4%	9.6%	0.8%	44
60	21.6%	43.2%	28.8%	6.4%	53
40	6.4%	28.8%	43.2%	21.6%	61

more pronounced in the rock containing 60% orthopyroxene. This mixture has a median dihedral angle of ~61°; nonetheless the calculated permeability is drastically different from the theoretical value of an isotropic system with equivalent dihedral angle (Fig. 6). The most significant reduction in permeability occurs at a melt fraction of ~0.02, which corresponds to the pinch-off of the ol–opx–opx junctions that make up 43.2% of the channels. Our results show that a melt fraction of 0.02 is required to form an interconnected melt network in a system with 60% orthopyroxene.

4. Discussion

4.1. Permeability–porosity relationship

By incorporating different dihedral angles into a network model, we are able to predict the permeability of partially molten rocks, taking the grain-scale heterogeneity of melt distribution into account. In this study, we focused on the hypothetical cases of olivine–orthopyroxene mixtures. Our simulation results suggest that while the best-fitting permeability–porosity relationship for a three-phase system with at least 80% olivine is $k \propto \phi^2$, the exponent of the power law increases from 2 to ~3 when the olivine content is reduced to 60% (Fig. 7) at melt fractions greater than 0.01. The increase in the power-law exponent reflects the loss of connectivity (melt channel pinch-off) with decreasing melt fraction. In the 60% olivine system, a decrease in the power-law exponent at melt fractions below 0.01 is observed. This suggests that if the connectivity of the melt channels remains constant, the shrinkage in the size of melt channels due to the decrease in melt fraction results in a permeability–porosity relationship of $k \propto \phi^2$ in partially molten systems. Interestingly, Cheadle [35] has calculated the equilibrium shape of melt network with various dihedral angles, and finds that the exponent of the power law increases from 2 to ~3 when melt fraction exceeds 0.03.

The observed permeability–porosity relationship of $k \propto \phi^2$ at constant connectivity in partially molten rocks is different from that resulting from

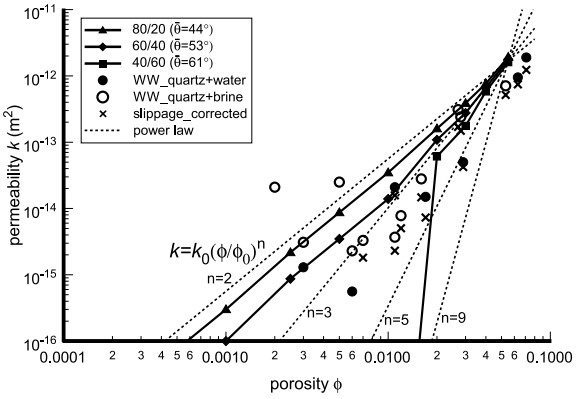

Fig. 7. Log–log plot of permeability data as a function of melt fraction in three-phase systems. The solid curves with triangles, diamonds and squares represent model results for an olivine+basalt system containing 20%, 40% and 60% orthopyroxene, respectively. The dashed lines are power-law relationships between permeability and porosity with different exponents ($n = 2$–9). For comparison, measured permeability data (normalized to grain diameter of 1 mm) for quartzite aggregates are also included [21,39]. The open circles are quartz+water experiments, and the filled circles are quartz+brine experiments.

diagenetic processes in sedimentary rocks. For example, Bourbié and Zinszner measured the permeability of Fontainebleau sandstone and obtained a permeability–porosity relationship of $k \propto \phi^3$ with porosities ranging from 7 to 28% [36]. Zhu et al. [27] pointed out that the permeability in Fontainebleau sandstones is more sensitive to porosity change because the pore-size distribution becomes more skewed toward the small size during porosity reduction. By contrast, as connectivity is constant in a partially molten rock, the reduction in melt channel size with decreasing melt fraction does not change the characteristics of the melt channel distribution. Therefore, more significant permeability reduction is observed only when the pinch-off occurs. In a system with further reduction in olivine content (to 40%, Fig. 7), a single power-law relationship does not capture the effects of a drastic loss in connectivity, and therefore is no longer applicable.

The network model provides a link between macroscopic physical properties and grain-scale melt distribution. Many factors, such as anisotropic interfacial energy, grain-size variation, de-

viatoric stress etc., can result in heterogeneous melt distribution. For example, in Wark and Watson's quartz+brine/water systems [21], the heterogeneity likely results from a combination of variations in grain size and anisotropic interfacial energies, which explains why the observed permeability–porosity relationship is different from the isotropic model predications.

4.2. Percolation threshold

The percolation threshold is defined as the critical occupation percentage of the conducting elements (melt channels) below which there is no interconnected flow path in the network. In our model, the percolation threshold is determined by the ratio of 'wetted' grain edges versus total grain edges, which is different from the critical melt fraction commonly used in mantle geochemistry. We calculate that the percolation threshold for the 3D tetrakaidekahedron network is ~39% (Fig. 8). In other words, at least 39% of the three grain junctions must be 'wetted' to form an interconnected melt network. This value agrees well with the percolation threshold for a 3D diamond lattice network given by Shante and Kirkpatrick [37], which is expected because both of the fact that the networks are three-dimensional, with a coordination number of 4.

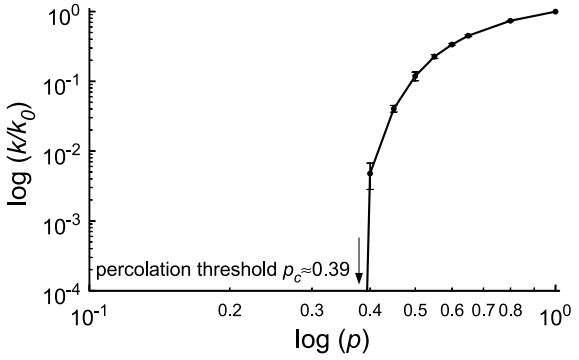

Fig. 8. Normalized permeability as a function of the occupation percentage of the conducting elements in a 3D tetrakaidekahedron network model. The percolation threshold of the network is approximately 0.39. The error bar marks the range of permeability values obtained from 10 different random networks. Note that the fluctuation is negligible until the network is at the percolation threshold.

In this study, we did not account for the grain-scale redistribution of melt caused by lithologic variations [38]. The redistribution of melt may further reduce the minimum cross-sectional C_{ch} of a melt channel with high dihedral angle. Toramaru and Fujii [18] observed that in partially molten peridotites containing olivine, orthopyroxene, and clinopyroxene and 7% melt, triple junctions of ol–ol–opx appeared melt-free. Therefore 'non-wetted' grain boundaries are more numerous in their samples than predicted in our model when we simply average the dihedral angles at each triple junction. For example, our model predicts all the triple junctions will be 'wetted' at melt fractions greater than 0.05. At melt fraction less than 2% (when pinch-off occurs), only 35.2% of the triple junctions in our model have dihedral angles larger than 60° in a rock with orthopyroxene content of 40%, which is above the percolation threshold of 39%. However, in the same rock with 40% orthopyroxene, there are 43.2% ol–ol–opx triple junctions. If we treat these triple junctions as melt-free as suggested by Toramaru and Fujii [18], the network is below the percolation threshold. In this case, the melt cannot percolate through the model and permeability would be drastically reduced (Fig. 8).

In a heterogeneous system, 'non-wetted' grain boundaries resulting from the anisotropic interfacial energy or the grain-scale redistribution of melt caused by lithologic variations are common. For example, Daines and Kohlstedt [19] observed the existence of melt-free ('non-wetted') triple junctions in the olivine and orthopyroxene mixture with 8% melt. However, experimental observations on the effect of the addition of orthopyroxene on melt transport remain ambiguous. Daines and Kohlstedt [19] measured melt migration profiles generated between a disc of olivine with 20% orthopyroxene plus 8% melt and a disc with 0–2% melt. Even though the existence of melt-free triple junctions for samples containing orthopyroxene leads to the expectation of a slower melt migration rate, their melt migration profiles actually show a slight enhancement in the melt migration rate for samples containing orthopyroxene compared to samples with only olivine. In conclusion, the grain-scale redistribution of

melt caused by lithologic variations may play an important role for melt transport; however, relatively few data are available from experimental and microstructural studies to provide quantitative constraints. Systematic laboratory experiments and quantitative microstructural analysis are needed before we can incorporate this effect into the current model.

5. Conclusions

We developed a 3D network model to estimate the permeability of a partially molten system with a heterogeneous melt distribution. In our model, each conducting channel is treated as a prism with a constant cross-sectional area and a length equal to that of the grain edge. The cross-sectional area of each prism is determined by a given dihedral angle and a local melt fraction. By incorporating different dihedral angles and local melt fractions into a 3D tetrakaidekahedral network, our model is an analog for a partially molten rock, and thus allows us to calculate permeability as a function of distributions of the dihedral angle and melt fraction. Important results of this study are summarized below.

1. A 3D network model for permeability and connectivity can be related directly to quantitative microstructural data of melt geometry. The combination of network modeling and detailed microstructural analysis will be a useful tool for estimating permeability and providing constraints on melt segregation/migration rates in partially molten systems.
2. Our results show that the permeability in partially molten rocks is sensitive to grain-scale heterogeneity resulting from non-uniform grain size, non-hydrostatic stresses, and anisotropic interfacial energy. The permeability of an olivine–basalt system containing $>40\%$ of orthopyroxene is significantly lower than that of a homogeneous partially molten rock with the same median dihedral angle, particularly at low melt fraction. Our results indicate that if the connectivity of the melt channels remains constant, the shrinkage in the size of melt channels due to the decrease in melt fraction results in a permeability–porosity relationship of $k \propto \phi^2$ in a partially molten rock. An increase in the power-law exponent occurs with the loss of melt channel connectivity.
3. By relating macroscopic permeability to the microscopic melt distribution, network modeling helps us understand the results of experimental studies. Our numerical approach also addresses the transport properties of low-porosity systems ($\phi < 0.1\%$) inaccessible to experiments yet important for interpreting geochemical and geophysical constraints on melting processes in the upper mantle.

Acknowledgements

W.Z. was supported by the Department of Energy through Grant DE-FG02-00ER15058 and the National Science Foundation through Grant NSF-EAR9814796. G.H. was supported through NSF Grant OCE-0099316. Reviews from Scott King, Michael Brown and Yan Liang helped to clarify the manuscript. *[SK]*

References

[1] C.S. Smith, Some elementary principles of polycrystalline microstructure, Metall. Rev. 9 (1964) 1–48.
[2] H.S. Waff, J.R. Bulau, Experimental studies of near-equilibrium textures in partially molten silicates at high pressure, Adv. Earth Planet. Sci. 12 (1982) 229–236.
[3] H.S. Waff, Effects of the gravitational field on liquid distribution in partial melts within the upper mantle, J. Geophys. Res. 85 (1980) 1815–1825.
[4] R.F. Cooper, D.L. Kohlstedt, Sintering of olivine and olivine-basalt aggregates, Phys. Chem. Miner. 11 (1984) 5–16.
[5] S.R. Jurewicz, E.B. Watson, The distribution of partial melt in a granitic system: The application of liquid phase sintering theory, Geochim. Cosmochim. Acta 49 (1985) 1109–1121.
[6] H.H. Park, D.N. Young, Effect of dihedral angle on the morphology of grains in a matrix phase, Metall. Trans. A 16 (1985) 923–928.
[7] N. von Bargen, H.S. Waff, Permeabilities, interfacial areas, and computations of equilibrium microstructures, J. Geophys. Res. 91 (1986) 9261–9276.
[8] H.S. Waff, U.H. Faul, Effects of crystalline anisotropic on

fluid distribution in ultramafic partial melts, J. Geophys. Res. 97 (1992) 9003–9014.
[9] U.H. Faul, Permeability of partially molten upper mantle rocks from experiments and percolation theory, J. Geophys. Res. 102 (1997) 10299–10311.
[10] W. Beere, A unifying theory of the stability of penetrating liquid phases and sintering pores, Acta Metall. 36 (1988) 469–491.
[11] J.R. Bulau, H.S. Waff, J.A. Tyburczy, Mechanical and theomodynamic constraints on fluid distribution in partial melts, J. Geophys. Res. 84 (1979) 6102–6108.
[12] C.F. Frank, Two-component flow model for convection in the earth's upper mantle, Nature 220 (1968) 350–352.
[13] S. Maaløe, A. Scheie, The permeability controlled accumulation of primary magma, Contrib. Mineral. Petrol. 81 (1982) 350–357.
[14] M.J. Cheadle, Properties of textually equilibrated two-phase aggregates, Ph.D. Thesis, Cambridge, 1989.
[15] D.L. Turcotte, G. Schubert, Geodynamics, Wiley, New York, 1982.
[16] P.J. Vaughan, D.L. Kohlstedt, H.S. Waff, Distribution of the glass phase in hot pressed, olivine-basalt aggregates: An electron microscopy study, Contrib. Mineral. Petrol. 81 (1982) 253–261.
[17] R.F. Cooper, D.L. Kohlstedt, Interfacial energies in the olivine-basalt system, Adv. Earth Planet. Sci. 12 (1982) 217–228.
[18] A. Toramaru, N. Fujii, Connectivity of melt phase in a partially molten peridotite, J. Geophys. Res. 91 (1986) 9239–9252.
[19] M.J. Daines, D.L. Kohlstedt, A laboratory study of melt migration, Philos. Trans. R. Soc. Lond. A 342 (1993) 43–52.
[20] U.H. Faul, D.R. Toomey, H.S. Waff, Intergranular basaltic melt is distributed in thin, elongated inclusions, Geophys. Res. Lett. 21 (1994) 29–32.
[21] D.A. Wark, E.B. Watson, Grain-scale permeabilities of texturally equilibrated, monomineralic rocks, Earth Planet. Sci. Lett. 164 (1998) 591–605.
[22] M. Spiegelman, T. Elliot, Consequences of melt transport for uranium series disequilibruim, Earth Planet. Sci. Lett. 109 (1993) 1–20.
[23] D. McKenzie, Some remarks on the movement of small melt fraction in the mantle, Earth Planet. Sci. Lett. 95 (1989) 53–72.
[24] The MELT Seismic Team, Imaging the deep seismic structure beneath a mid-ocean ridge: the MELT experiment, Science 280 (1998) 1215–1218.
[25] D. McKenzie, Constraints on melt generation and transport from U-series activity ratios, Chem. Geol. 162 (2000) 81–94.
[26] C. David, Y. Guéguen, G. Pampoukis, Effective medium theory and network theory applied to the transport properties of rocks, J. Geophys. Res. 95 (1990) 6993–7005.
[27] W. Zhu, C. David, T.-f. Wong, Network modeling of permeability evolution during cementation and hot isostatic pressing, J. Geophys. Res. 100 (1995) 15451–15464.
[28] W. Zhu, B. Evans, Y. Bernabé, Densification and permeability reduction in hot-pressed calcite: A kinetic model, J. Geophys. Res. 104 (1999) 25501–25511.
[29] W. Zhu, T.-f. Wong, Network modeling of the evolution of permeability and dilatancy in compact rock, J. Geophys. Res. 104 (1999) 2963–2971.
[30] P.M. Doyen, Permeability, conductivity, and pore shape evolution of sandstone, J. Geophys. Res. 93 (1988) 7729–7740.
[31] F.A.L. Dullien, Porous Media: Fluid Transport and Pore Structure, Academic Press, San Diego, CA, 1992.
[32] Y. Guéguen, J.K. Dienes, Transport properties of rocks from statistics and percolation, Math. Geol. 21 (1989) 1–13.
[33] C. Herring, Some theorems on the free energies of crystal surfaces, Phys. Rev. 82 (1951) 87–93.
[34] D. Laporte, A. Provost, Equilibrium geometry of a fluid phase in a polycrystalline aggregate with anisotropic survey energies; dry grain boundaries, J. Geophys. Res. 105 (2000) 25937–25953.
[35] M. Cheadle, Properties of textually equilibrated two-phase aggregates, Ph.D. Thesis, Cambridge, 1989.
[36] T. Bourbié, B. Zinszner, Hydraulic and acoustic properties as a function of porosity in Fontainebleau sandstone, J. Geophys. Res. 90 (1985) 11524–11532.
[37] V.K.S. Shant, S. Kirkpatrick, An introduction to percolation theory, Adv. Phys. 20 (1971) 325–357.
[38] E.B. Watson, Lithogic partitioning of fluids and melts, Am. Mineral. 84 (1999) 1693–1710.
[39] Y. Liang, J.D. Price, D.A. Wark, E.B. Watson, Nonlinear pressure diffusion in a porous medium: Approximate solutions with applications to permeability measurements using transient pulse decay method, J. Geophys. Res. 106 (2001) 529–535.